Supporting Information for:

Nickel Metal Nanoparticles as Anode Electrocatalyst for Highly-Efficient Direct Borohydride Fuel Cells

Alexandr G. Oshchepkov[a,b,*], Guillame Braesch[a,c], Salem Ould-Amara[d], Gholamreza Rostamikia[e], Gaël Maranzana[d], Antoine Bonnefont[f], Vasiliki Papaefthimiou[a], Michael J. Janik[e], Marian Chatenet[c,*], Elena R. Savinova[a]

[a] *Institut de Chimie et Procédés pour l'Energie, l'Environnement et la Santé, UMR 7515 CNRS-University of Strasbourg, 67087 Strasbourg Cedex, France*
[b] *Boreskov Institute of Catalysis, 630090 Novosibirsk, Russia*
[c] *University Grenoble Alpes, University Savoie Mont Blanc, CNRS, Grenoble INP, LEPMI, 38000 Grenoble, France*
[d] *Université de Lorraine, CNRS, LEMTA, UMR 7563, 54504 Vandoeuvre Les Nancy, France*
[e] *Department of Chemical Engineering, Pennsylvania State University, University Park, PA, 16802, USA*
[f] *Institut de Chimie de Strasbourg, UMR 7177 CNRS-University of Strasbourg, 67070 Strasbourg, France*

Analysis of the Ni_{ED}/C and Ni_{ED}/GDE electrodes for possible Pt contamination.

The composition of Ni nanoparticles deposited on either XC-72R carbon (Ni_{ED}/C) or SGL carbon cloth (Ni_{ED}/GDE) was analyzed by X-ray Energy-dispersive spectroscopy (X-EDS) combined with either Transmission Electron Microscopy (TEM) or Scanning Electron Microscopy (SEM). Figures S1 and S2 show a typical TEM or SEM micrographs of the Ni_{ED}/C and Ni_{ED}/GDE samples, respectively, along with the corresponding X-EDS analyses from the highlighted areas. The expected positions of Pt peaks are also highlighted for clarity to ensure the absence of any Pt contamination on the surface of the Ni_{ED}/C and Ni_{ED}/GDE samples after the synthesis.

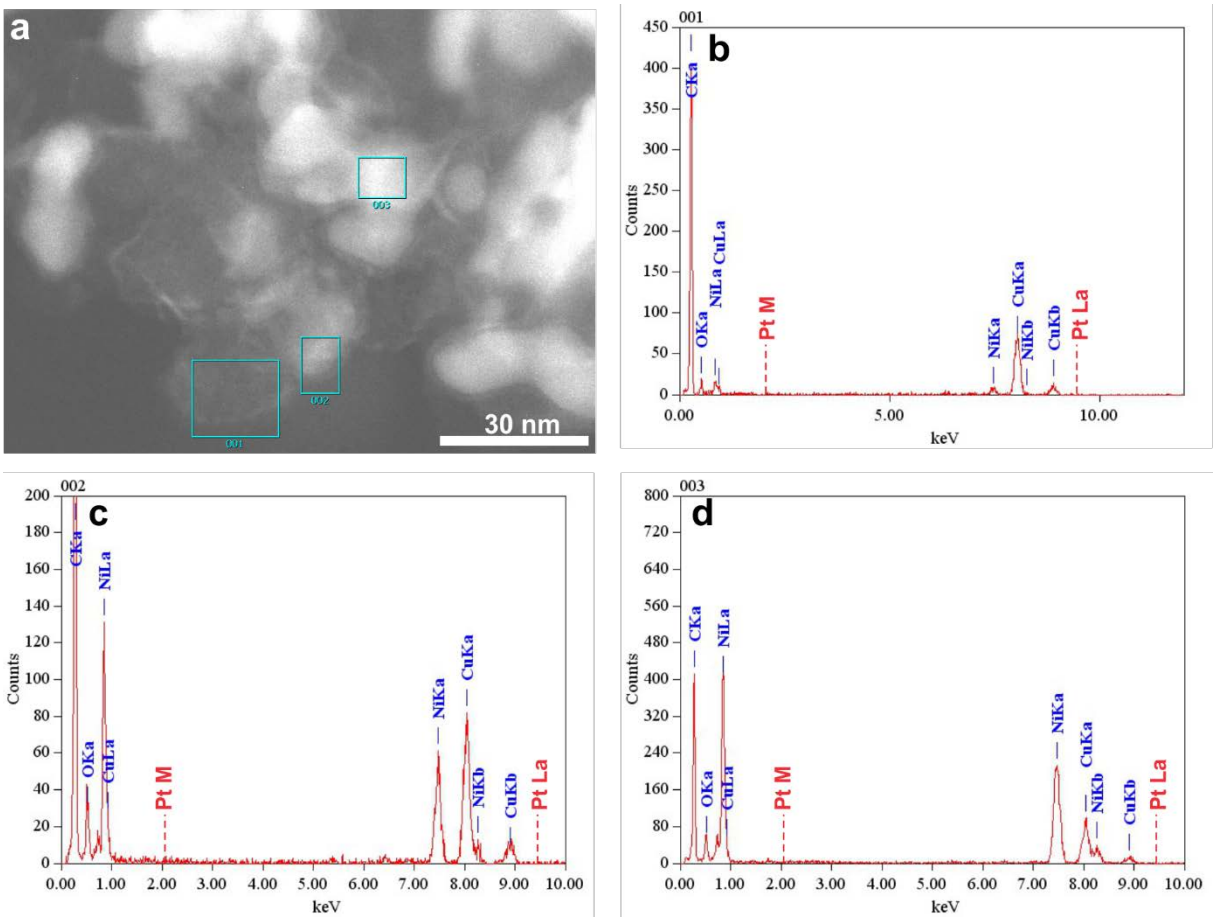

Figure S1. (a) TEM image of Ni_{ED}/C sample and corresponding X-EDS analyses from the marked areas (b) 001, (c) 002, (d) 003.

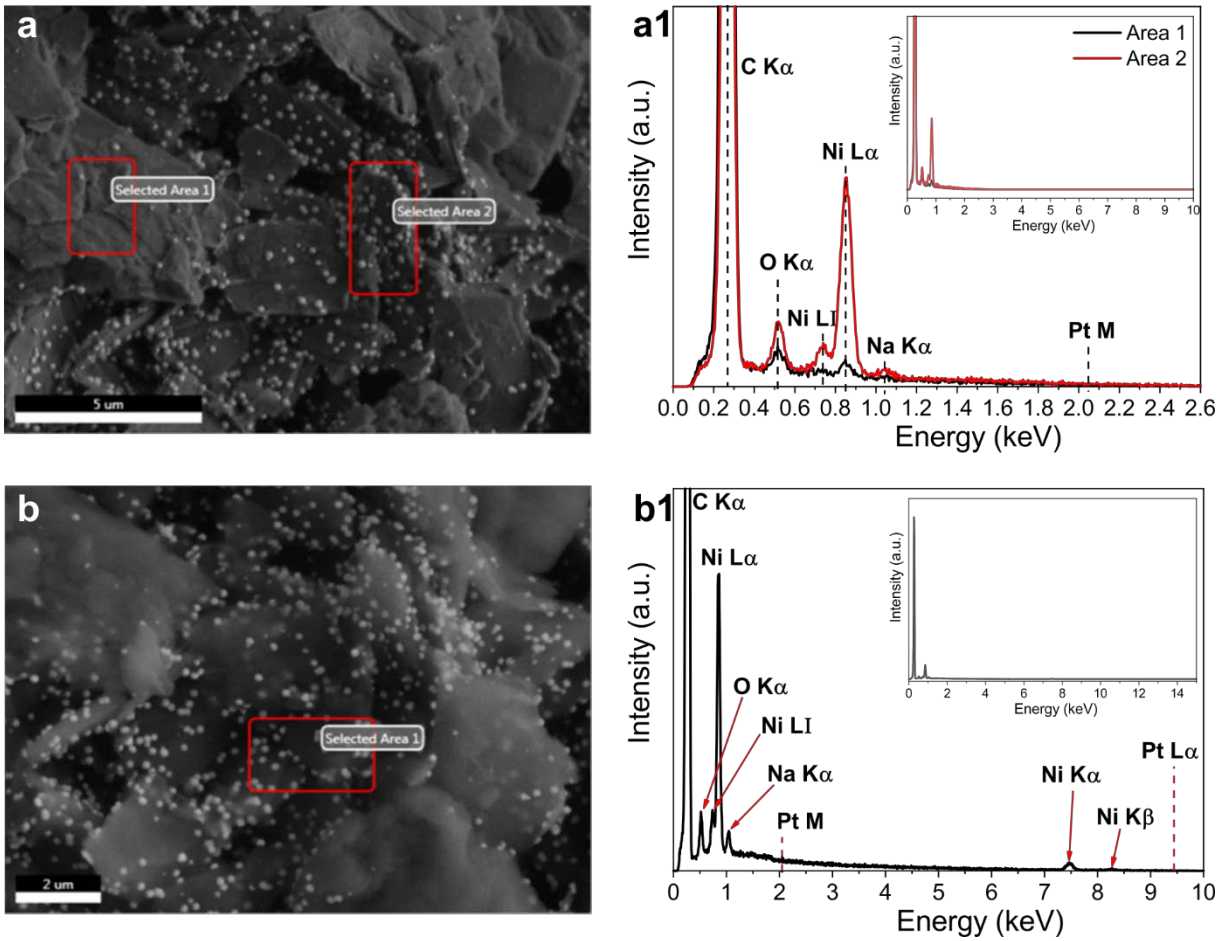

Figure S2. SEM images of Ni_{ED}/GDE-L sample obtained at (a) 3 or (b) 10 kV and corresponding X-EDS analyses from the marked areas (a1, b1).

The most active sample, *i.e*. metallic Ni_{ED}/C was also studied by XPS after the potentiostatic measurements of borohydride oxidation presented on Fig. 2c from the main text of the manuscript. Before the measurement, the electrode (GC disk with supported Ni_{ED}/C electrocatalyst) was thoroughly rinsed with water to remove any trace of NaOH and $NaBH_4$ electrolyte from its surface and dried under N_2 flow. Then the electrode was placed in the XPS chamber as is (without scratching the catalyst layer). Figure S3 shows a survey spectrum along with magnified areas around the binding energies of Pt ($4f_{7/2}$ – 71 eV, $4f_{5/2}$ – 74 eV, $4d_{5/2}$ – 315 eV, $4d_{3/2}$ – 332 eV, $4p_{3/2}$ – 520 eV)[1]. As can be clearly seen from Figures S3b - d, absolutely no Pt features can be found on the spectrum, revealing the absence of Pt contamination after the BOR test.

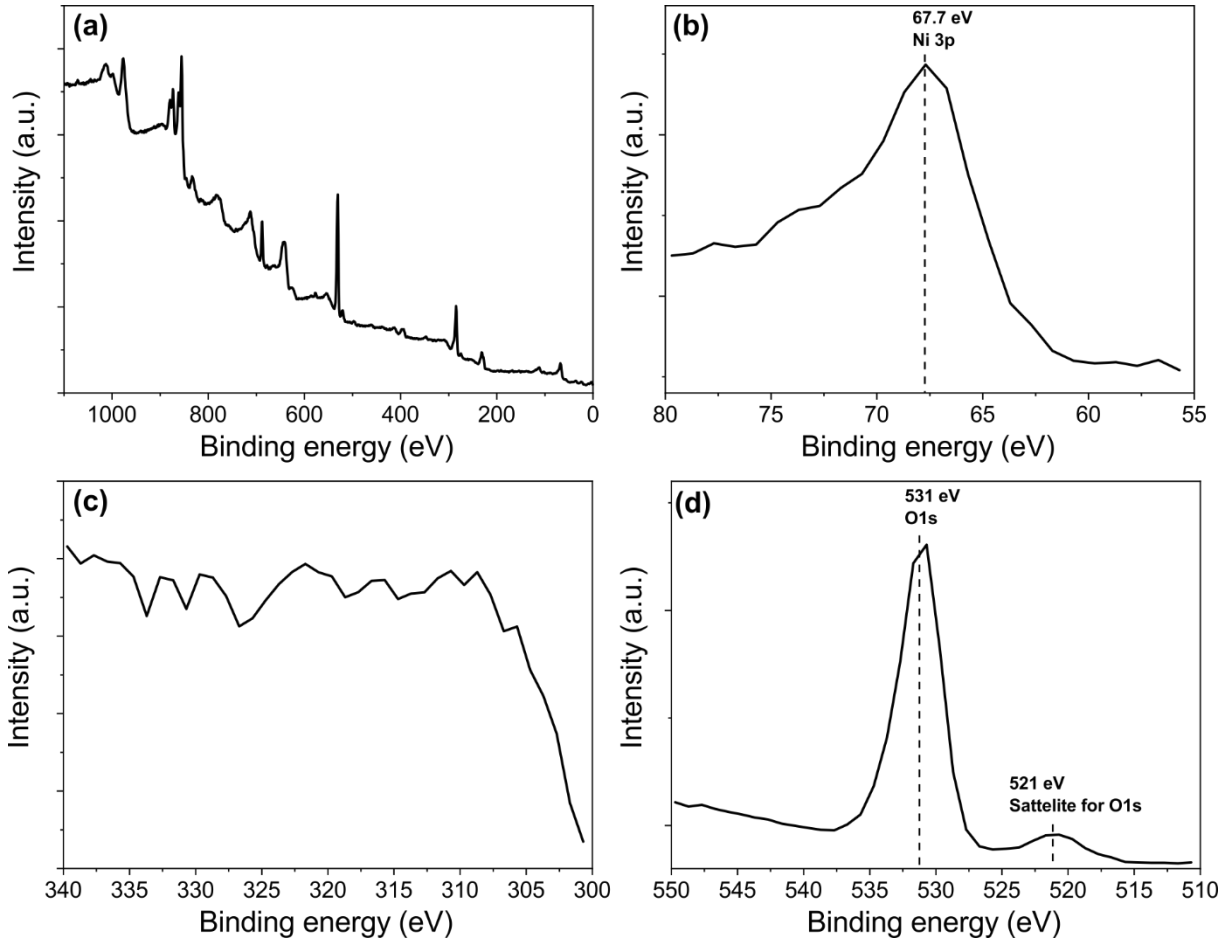

Figure S3. (a) Survey XPS spectrum obtained for metallic Ni_{ED}/C electrode after potentiostatic measurements in 1.0 M NaOH + 5 mM $NaBH_4$, at ω = 1600 rpm and E = 0.1 V vs RHE. Panels (b), (c) and (d) magnify the areas where 4f, 4d and 4p peaks of Pt, respectively, might be expected.

Preparation of the Ni_{ED}/C catalyst with various state of the electrode surface

To explore the influence of surface oxide species on electrochemical and electrocatalytic properties of Ni_{ED}/C, three states of its surface were considered. In the first case, the experiments were performed immediately after the preparation of the sample and quick rinsing of the electrode by water (to remove the Ni salt left on the surface after electrodeposition). Such electrodes represent metallic state of the Ni surface, substantially free from oxide species. In the second and third cases, before conducting the measurements, the Ni_{ED}/C electrodes were rinsed by water and then subjected to surface-oxidation in supporting 1.0 M NaOH electrolyte. The latter was done electrochemically by either applying potential of E = 1.0 V *vs* RHE for 5 minutes or recording 5 consecutive scans between E = -0.2 V *vs* RHE and E = 1.6 V *vs* RHE at v = 20 mV s^{-1}. These corresponding electrodes represent a partially- or strongly-oxidized state of the Ni_{ED}/C electrode surface, respectively. Prior to the addition of the borohydride solution to the electrolyte, the Ni_{ED}/C electrodes were conditioned in 1.0 M NaOH between E = -0.2 V *vs* RHE and E = 0.4 V *vs* RHE until stabilization of the CV profile. After that, the electrochemical surface area was evaluated by acquiring CVs in the potential interval from E = -0.06 to 0.40 V *vs* RHE (Figure S4) and considering the entire value of the anodic charge and the 0.514 mC cm^{-2} conversion coefficient [2].

Electrochemical characterizations

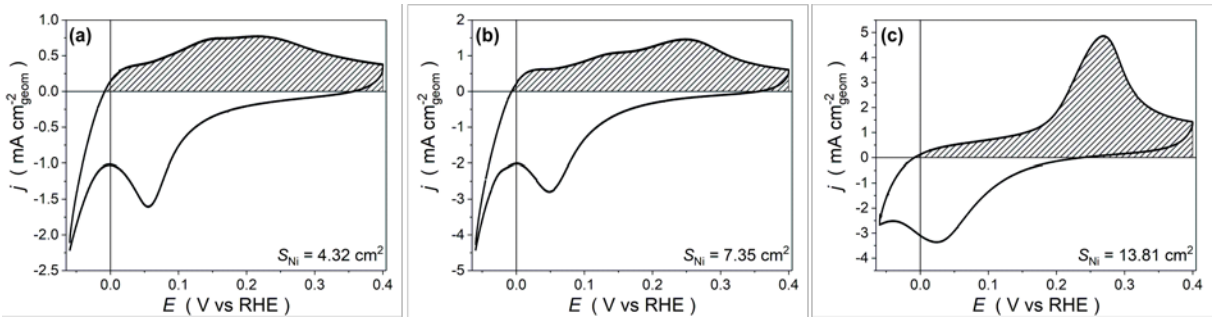

Figure S4 CV curves for (a) strongly-oxidized, (b) partially-oxidized and (c) metallic Ni_{ED}/C obtained in N_2-saturated 1.0 M NaOH at v = 20 mV s^{-1}. The patterned area of the CVs was integrated to estimate the electrochemical surface area of Ni.

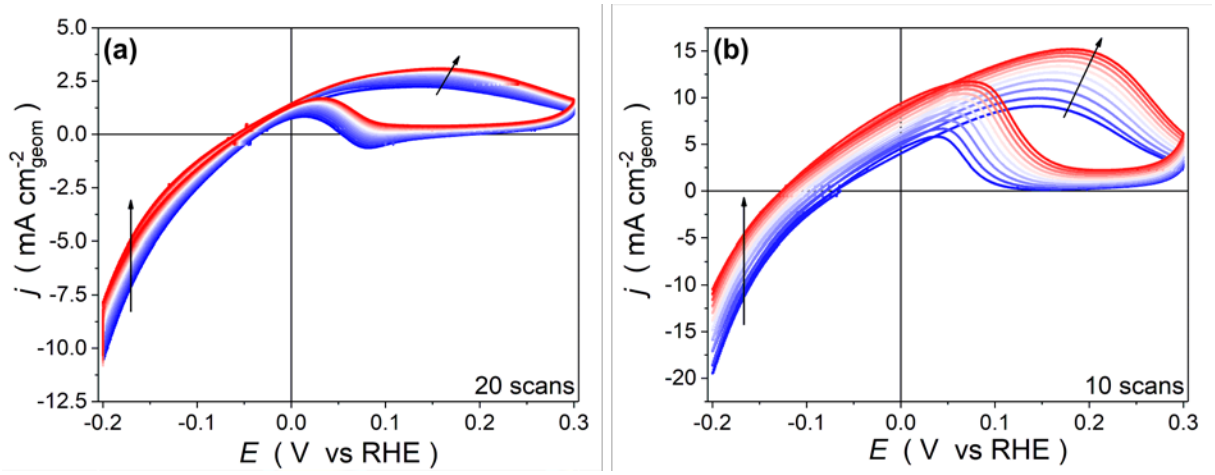

Figure S5 Evaluation of CV curves obtained for (a) strongly-oxidized and (b) partially-oxidized Ni_{ED}/C in N_2-saturated 5 mM $NaBH_4$ + 1.0 M NaOH at v = 20 mV s^{-1}.

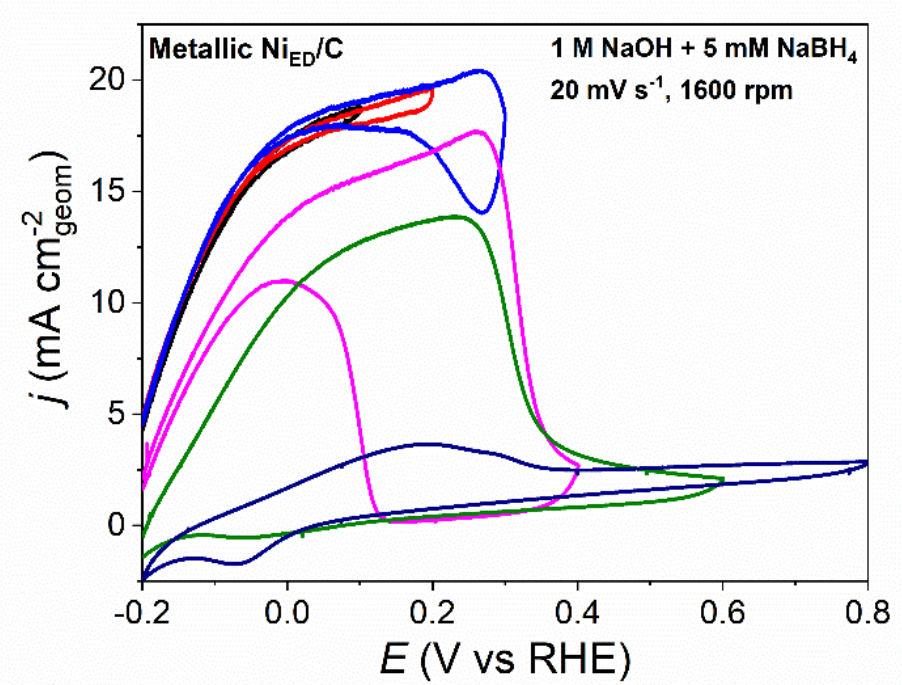

Figure S6 CV curves obtained for metallic Ni_{ED}/C under N_2 atmosphere in 1.0 M NaOH + 5 mM $NaBH_4$ at v = 20 mV s^{-1}, ω = 1600 rpm and various anodic potential limit (0.1, 0.2, 0.3, 0.4, 0.6, 0.8 V *vs* RHE).

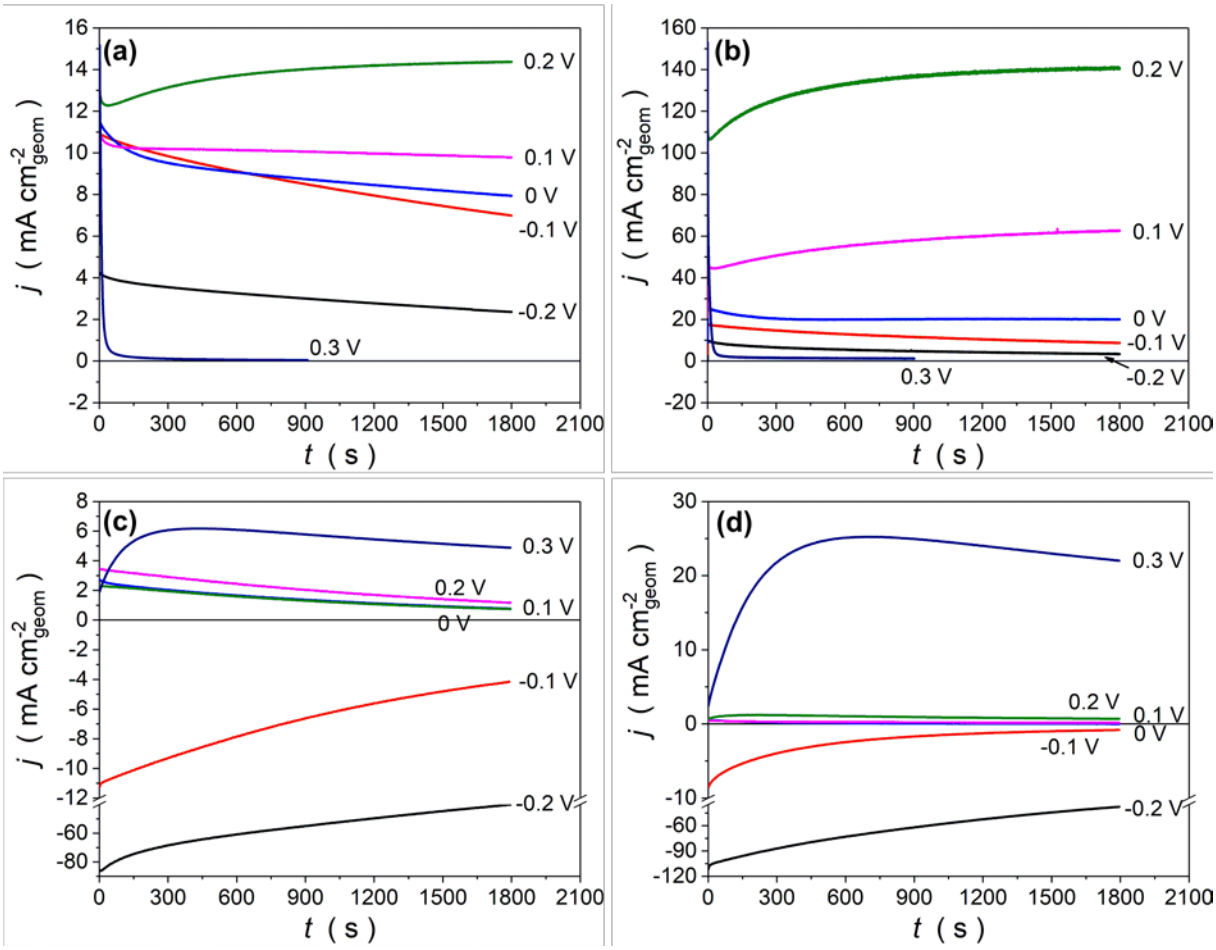

Figure S7 Potentiostatic measurement of the (a, b) Ni_{ED}/C and (c, d) Pt/C electrodes in N_2-saturated 1.0 M NaOH + 5 (a, c) or 50 (b, d) mM $NaBH_4$ electrolyte (ω = 1600 rpm; -0.2 < E < 0.3 V *vs* RHE).

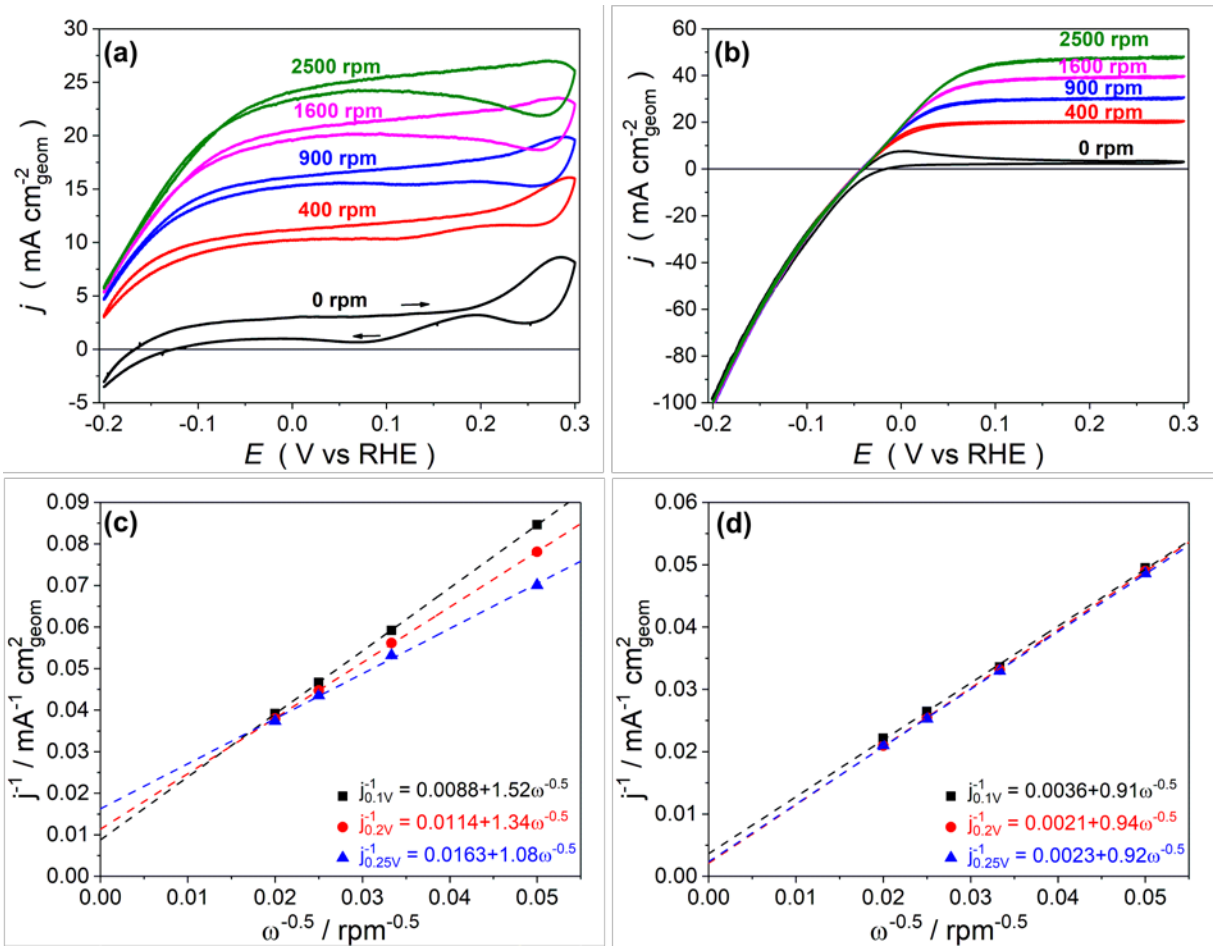

Figure S8 CV curves obtained for (a) Ni_{ED}/C and (b) Pt/C using rotating disk electrode in N_2-saturated 1.0 M NaOH + 5 mM $NaBH_4$ electrolyte at v = 20 mV·s^{-1} and various rotation speeds. (c, d) Corresponding Koutecky-Levich plots at various potentials.

The rotating rate dependence of the RDE polarization curves has been analyzed using Koutecky-Levich equation:

$$j^{-1} = j_k^{-1} + j_d^{-1} = j_k^{-1} + B^{-1}\omega^{-0.5}$$

where j_k and j_d correspond to kinetic and diffusion-limited current density, respectively.

The Koutecky-Levich plots for Pt/C electrode (Figure S7d) almost cross 0, showing that the limiting currents are established at potentials above 0.1 V *vs* RHE. On the contrary for Ni_{ED}/C sample, a significant deviation from an expected line is observed (Figure S7c) likely due to a change of the number of released electrons of the BOR at different potentials.

The slope B can be calculated according to the Levich equation as:

$$B = 0.62 \cdot nD^{\frac{2}{3}}Fv^{-\frac{1}{6}}C_0,$$

where n is a number of involved electrons in the BOR, F is the Faraday constant (96485 C mol^{-1}), C_0 is the concentration of the $NaBH_4$ in 1.0 M NaOH (*i.e.* 5 mM), D is the the diffusion coefficient of BH_4^- ($2.6 \cdot 10^{-5}$ cm^2 s^{-1} [3]), v is the kinematic viscosity of the electrolyte (0.0118 cm^2 s^{-1} [3]). Thus the theoretical values of the B are calculated to be 2.81, 1.40, 0.94, 0.70 at the release of 2, 4, 6 and 8 electrons in the BOR,

respectively. Therefore, analysis of the Koutecky-Levich plots presented on Figures S7c, d shows that the number of released electrons is close to 4 and 6 for Ni_{ED}/C and Pt/C catalysts, respectively.

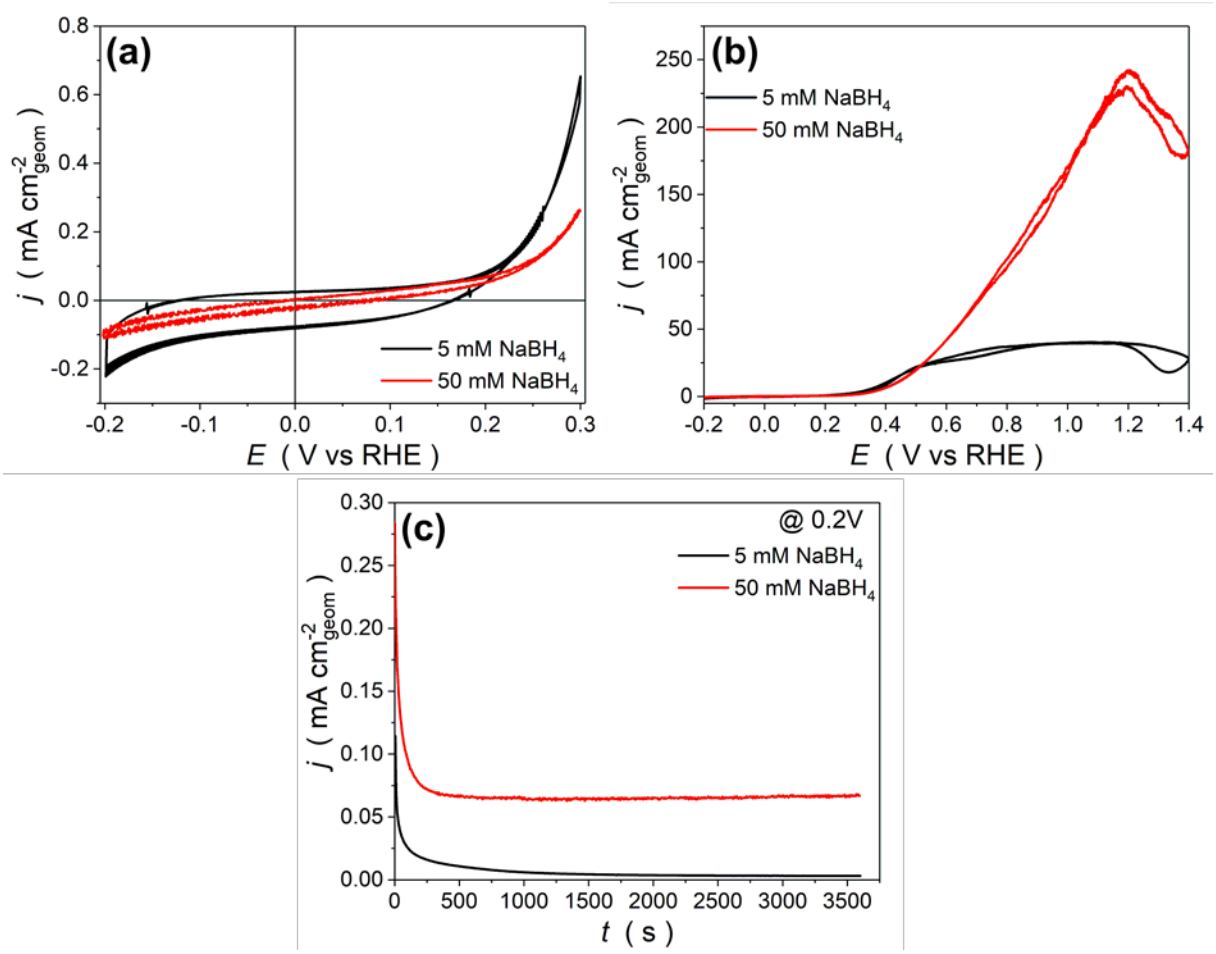

Figure S9 (a, b) CV curves obtained for Au/C in N_2-saturated 1.0 M NaOH + 5 (black curve) or 50 (red curve) mM $NaBH_4$ at v = 20 mV s^{-1} and ω = 1600 rpm. (c) Potentiostatic measurement of the corresponding electrode in N_2-saturated 1.0 M NaOH + 5 or 50 mM $NaBH_4$ electrolyte (ω = 1600 rpm; E = 0.2 V *vs* RHE).

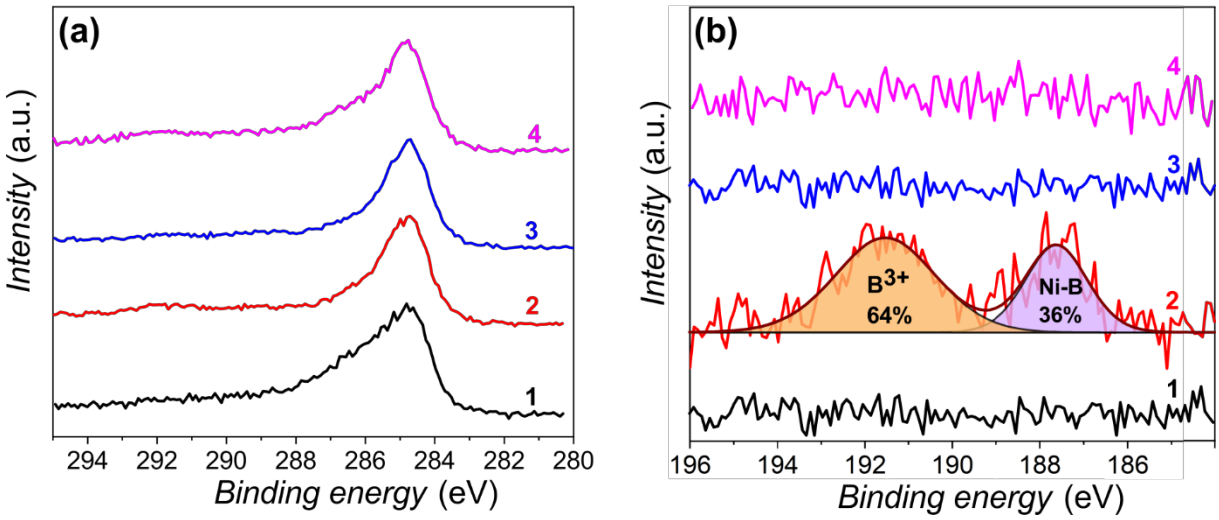

Figure S10. (a) C 1s and (b) B 1s X-Ray photoelectron spectra obtained for metallic (1, 2) and strongly-oxidized (3, 4) Ni_{ED}/C samples after their treatment in either 1 M NaOH (1, 3) or 1 M NaOH + 50 mM $NaBH_4$ (2, 4). B 1s spectrum of metallic NiED/C samples after potentiostatic treatment (at E = 0.1 V vs RHE for 15 min) in 1 M NaOH + 50 mM $NaBH_4$ was curve-fitted with Ni-B (blue) and B^{3+} (green) components based on the literature data [4–6].

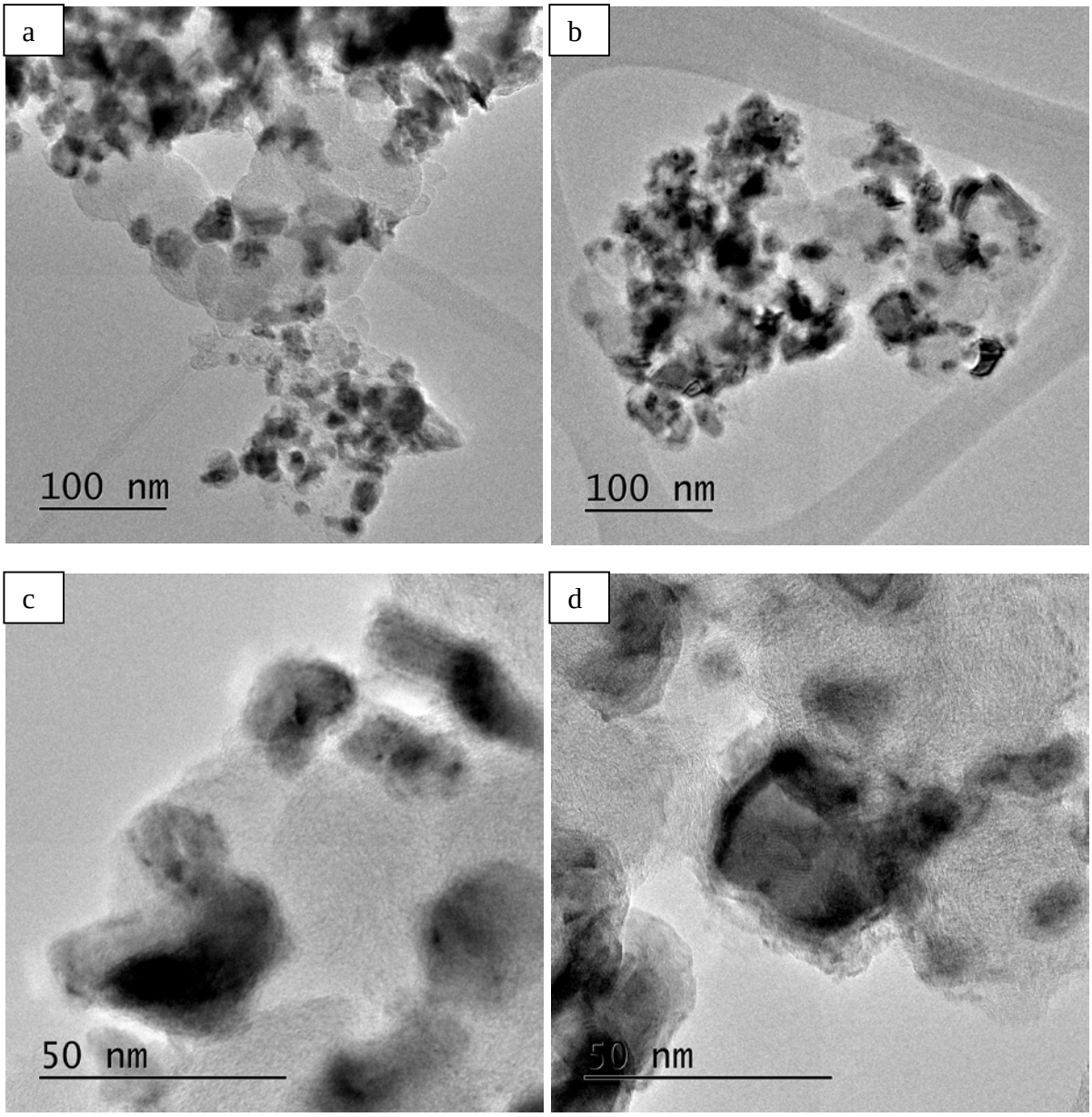

Figure S11 Representative TEM images of the Ni_{ED}/C nanoparticles upon their synthesis by electrodeposition (a, c) and after BOR characterizations (b, d).

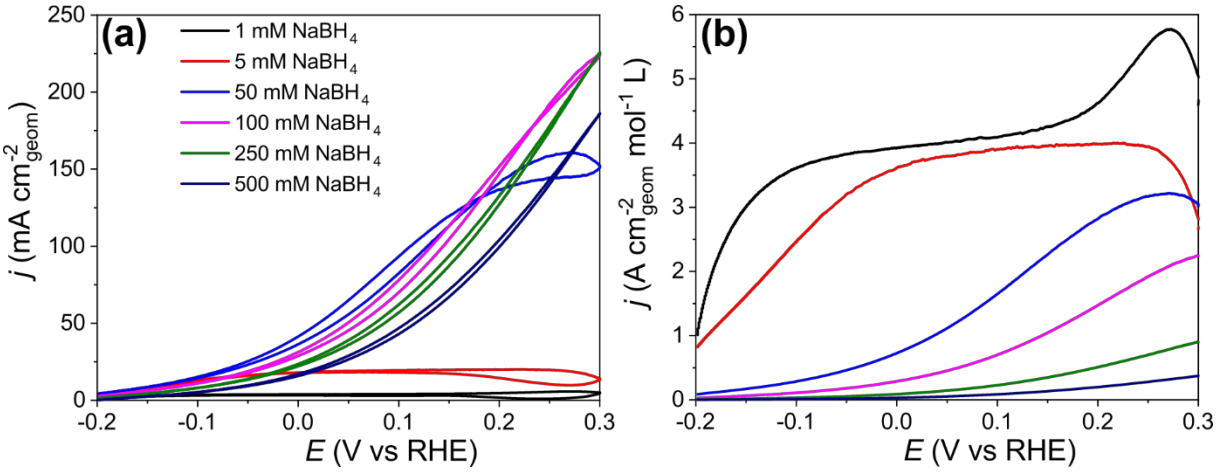

Figure S12. CV curves obtained for metallic Ni_{ED}/C under N_2 atmosphere in 1.0 M NaOH and various concentrations of $NaBH_4$, v = 20 mV s^{-1}, ω = 1600 rpm

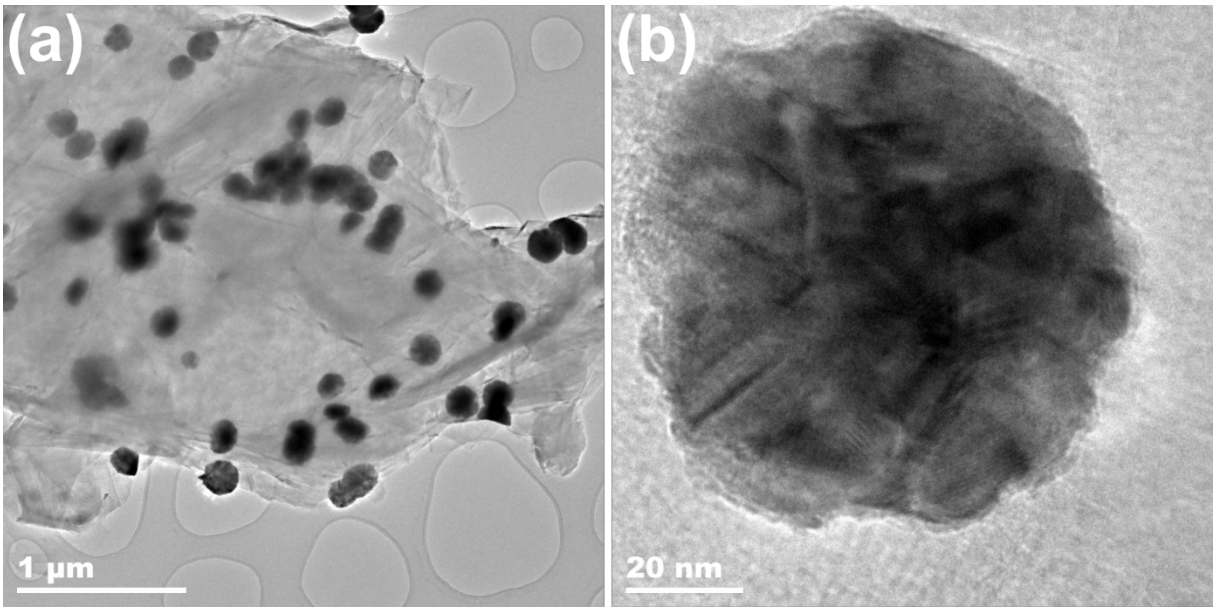

Figure S13. TEM (a) and HRTEM (b) images of the Ni_{ED}/GDE-L nanoparticles. Too high size of Ni particles prevents from the detailed analysis by TEM, although the nanostructured nature of the particle is clearly seen.

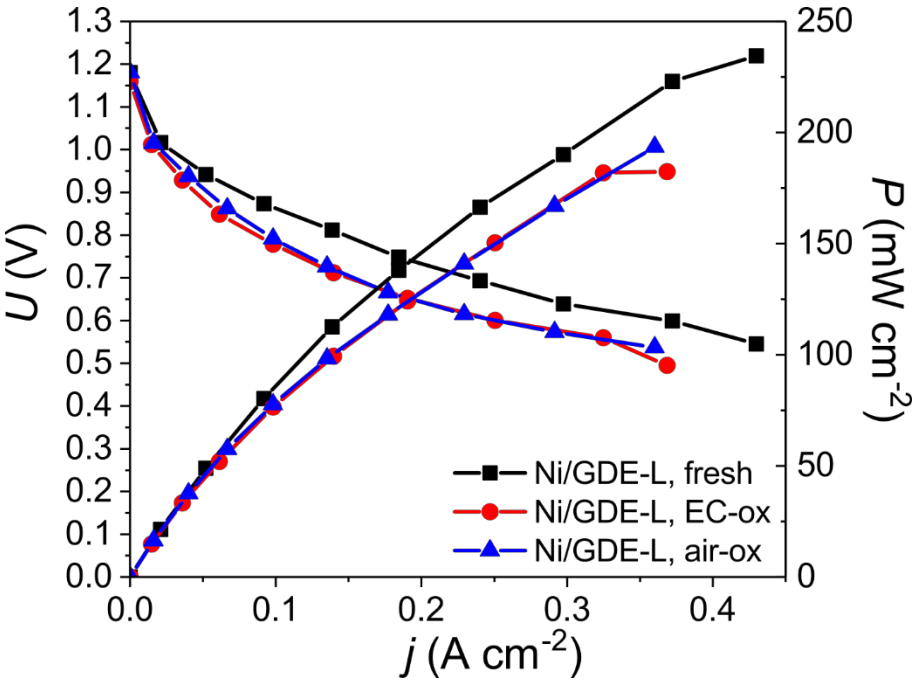

Figure S14. Ohmic-drop corrected *I-U* and *I-P* curves obtained in unit fuel cell configuration using Ni_{ED}/GDE-L anodes and Pt-black/GDE cathode, 0.50 M $NaBH_4$ + 4.0 M NaOH, pure oxygen. 'Fresh' sample was introduced in the DBFC right after the preparation; 'EC-ox' sample was first subjected to electrochemical oxidation by applying E = 1.0 V vs RHE for 3 min in 1.0 M NaOH electrolyte; 'Air-ox' sample was kept under contact with air for few days before being studied.

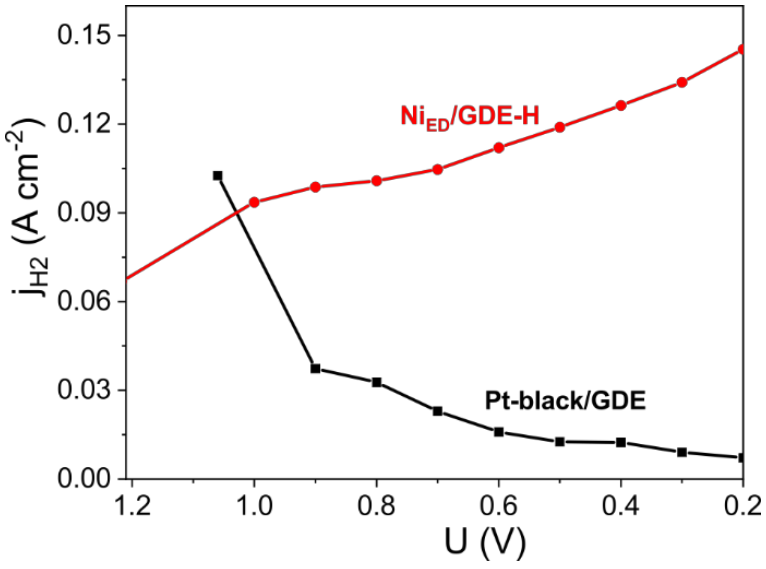

Figure S15. Variation of the H_2 current densities measured by a PEMFC operating in hydrogen pump mode at 0.6 V, positioned downstream the unit DBFC – the results are presented as a function of the DBFC cell voltage.

Table S1 Atomic ratios of Ni, O, C, B in the studied Ni_{ED}/C samples

Sample	O, %	Ni, %	C, %	B, %
Strongly-oxidized Ni_{ED}/C after 1 M NaOH + 50 mM $NaBH_4$	28.6	16.6	54.8	0
Strongly-oxidized Ni_{ED}/C after 1 M NaOH	24.2	12.4	63.4	0
Metallic Ni_{ED}/C after 1 M NaOH + 50 mM $NaBH_4$	29.6	14.6	51.9	3.9
Metallic Ni_{ED}/C after 1 M NaOH	22.4	11.9	65.7	0

Quantitative calculations were performed using the XPS peak areas. The % surface ratio of all elements of the 4 samples was calculated by using the area of the core level peaks, normalized to the photoemission cross section by assuming a homogeneous distribution arrangement model.

Table S2. Review of electrochemical performances in the BOR. Symbols: *C* is the concentration, S_{geom} is the geometric surface area of the electrode, *ECSA* is the electrochemically active surface area, *T* is the temperature, ω is the rotation rate, *j* is the current density at specified potential *E*, *v* is the cycling voltammetry sweep rate.

Catalyst	Loading, mg cm$^{-2}_{met}$	C_{NaBH4}, mM	S_{geom}, cm^2	*ECSA*, m^2 g^{-1}	*T*, ^{o}C	ω, rpm	Chronoamperometry		Cyclic Voltammetry							Ref.
							j, mA cm$^{-2}_{geom}$ [*E*, V *vs* RHE]	*i*, A g$^{-1}_{met}$ [*E*, V *vs* RHE]	*v*, mV s^{-1}	*j*, mA cm$^{-2}_{geom}$ [*E*, V *vs* RHE]			*i*, A g$^{-1}_{met}$ [*E*, V *vs* RHE]			
										0	0.1	0.3	0	0.1	0.3	
Metallic Nied/C	0.087	50	0.196	85.6	25	0			20	35.2	42.3	56.1	405	486	645	This work
						1600	166 [0.2]	1908.3 [0.2]		101	156	187	1160	1796	2151	
	0.075	5		93.4			19.6 [0.1]	259.7 [0.1]		20.7	21.6	23.3	274	286	309	
Partially oxidized Nied/C	0.071	5		86.8			13.3 [0.1]	185.8 [0.1]		8.8	13.4	6.2	116	178	81.7	
Strongly oxidized Nied/C	0.085	5		76.2			1.8 [0.1]	20.8 [0.1]		1.4	2.9	1.6	19.0	38.1	21.7	
Ni@MWCNTs / Ni Sponge	18	50	1	-	r.t.	0	220 [0.34]	12.2 [0.34]		74	120	226	4.1	6.7	12.6	[7]
		100					320 [0.34]	17.8 [0.34]								
$Ni_{62.1}Cu_{37.9}$-90 foam	6.4	30	1	-	25	0	13.8 [0.08]	2.2 [0.08]	25	15	21	30	2.3	3.3	4.7	[8]
							17.1 [0.18]	2.7 [0.18]								
$Ni_{67.9}Cu_{38.1}$-180 foam	16.4						18.2 [0.08]	1.1 [0.08]								
							22.6 [0.18]	1.4 [0.18]								
Ni-Ru/C	-	190	0.8	-	25	0	49.3 [0.06]									[9]
Ni-Ru-F/C							68.4 [0.06]	20.7 [0.06]								
G-Co	0.36	50	0.785	26	25	0			10	-	0.8	3.1	-	2.3	8.7	[10]
G-Ni	0.19			31.2						1. 6	4.4	6.8	8.2	23.2	35.5	
G-Co-Ni (4.5:1:1)	0.24			518.6						35.2	55.9	100	147	233	417	
Ni/C	0.177	200	0.283	-	20	1600			50	8.5	15.5	43.1	47.9	87.8	243.6	[11]
Ni37-Pt3/C										9.7	18.0	50.2	54.9	102	284	
$Cu_{51}Ni_{37}Pd_{12}$@ Ni foam	0.207	50	1	196.4 (for Pd)	r.t.	0			20	6.5	18.3	60	31.4	88.4	290	[12]

Table S3. Review of DBFC performances. Symbols: *T* is the operating temperature, *S* is the geometric active surface area, *P* is the power density (not necessarily the maximum value, depending on the information available) obtained at the current density *j*.

Anode composition	Cathode composition	Separator	Anodic fuel	Cathodic fuel	*T*, ºC	S_{geom}, cm^2	*P* (mW cm^{-2}) [*j* (mA cm^{-2})]	Mass activity basis (W g^{-1}_{anode})	Ref.
Ni_{ED}/GDE-L (0.60 mg_{Ni} cm^{-2}) + Nafion®	Pt-black (2 mg_{Pt} cm^{-2})	NRE212	0.5 M $NaBH_4$ + 4.0 M NaOH	O_2	60	8	235 [430]	391.7	This work
Ni_{ED}/GDE-H (3.6 mg_{Ni} cm^{-2}) + Nafion®							243 [425]	67.5	
Pt-black/GDE (2 mg_{Pt} cm^{-2}) + Nafion®							88.3 [190]	44.2	
Ni powder (70 mg_{Ni} cm^{-2}) + PTFE, on Ni foam	$LaNi_{0.9}Ru_{0.1}O_3$ (7.5 mg cm^{-2})	PFM	0.8 M KBH_4 + 6 M KOH	O_2	r.t.	1	93 [120]	1.3	[13]
Ni-B powder (70 mg_{NiB} cm^{-2}) + PTFE, on Ni foam							180 [400]	2.6	
Ni (3.68 mg_{Ni} cm^{-2}) + Pd/C (0.13 mg_{Pt} cm^{-2}) + Nafion®, on Ni foam	Pt/C (1 mg_{Pt} cm^{-2})	N212	5 wt% $NaBH_4$ + 10 wt% NaOH	O_2	60	5	448 [900]	117.6	[14]
Ni (3.68 mg_{Ni} cm^{-2}) + Pd/C (0.13 mg_{Pt} cm^{-2}) + CCH, on Ni foam		CS					685 [1400]	179.8	
Ni (3.68 mg_{Ni} cm^{-2}) + Pd/C (0.13 mg_{Pt} cm^{-2}) + CCH, on Ni foam	Pt/C (1 mg_{Pt} cm^{-2})	CS	5 wt% $NaBH_4$ + 10 wt% NaOH	O_2	70	5	810 [1680]	212.6	[15]
Ni powder (0.96 mg_{Ni} cm^{-2}) + Pd/C (0.04 mg_{Pd} cm^{-2}) + Nafion®	Pt/C (1 mg_{Pt} cm^{-2})	N212	5wt% $NaBH_4$ + 10 wt% NaOH	O_2	60	5	237 [575]	237.0	[16]
Ni powder (0.96 mg_{Ni} cm^{-2}) + Pt/C (0.04 mg_{Pt} cm^{-2}) + Nafion®							270 [600]	270.0	
Ni powder (4.8 mg_{Ni} cm^{-2}) + Pd/C (0.2 mg_{Pd} cm^{-2}) + Nafion®							261 [600]	261.0	
Ni/C (1.0 mg_{Ni} cm^{-2}) + Nafion®	Pt/C (1 mg_{Pt} cm^{-2})	N212	5wt.% $NaBH_4$ + 10 wt.% NaOH	O_2	60	5	150.6 [340]	150.6	[11]
Ni37-Pt3/C (1.0 mg cm^{-2}) + Nafion®							221 [500]	221.0	
Ni35-Pt5/C (1.0 mg cm^{-2}) + Nafion®							212.5 [500]	212.5	
Ni30-Pt10/C (1.0 mg cm^{-2}) + Nafion®							210 [500]	210.0	
Pt/C (1.0 mg_{Pt} cm^{-2}) + Nafion®							106.3 [232]	106.3	
Ni powder (14.4 mg_{Ni} cm^{-2}) + … Pd/C (0.6 mg_{Pd} cm^{-2}) + PTFE, on Ni foam	Pt/C (1 mg_{Pt} cm^{-2})	N112	10% $NaBH_4$ + 20% NaOH	Air	60	100	180 [340]	12.0	[17]

Pd/C (0.6 mg_{Pd} cm^{-2}) + Nafion®, on Ni foam							240 [430]	16.0	
Ni powder (0.6 mg_{Ni} cm^{-2}) + Nafion®, on Ni foam							180 [430]	12.0	
Au/C (0.6 mg_{Pd} cm^{-2}) + Nafion®, on Ni foam							190 [430]	12.7	
Ag/C (0.6 mg_{Pd} cm^{-2}) + Nafion®, on Ni foam							205 [430]	13.7	
Ni/C (2 mg_{Ni} cm^{-2}) + Nafion®	Pt/C (2 mg_{Pt} cm^{-2})	N117	5 wt% $NaBH_4$ + 10 wt% NaOH	O_2	85	4	41 [75]	20.5	[18]
Ni powder (167 mg_{Ni} cm^{-2}), on Ni foam	Pt/C (1 mg_{Pt} cm^{-2})	NRE211	5% $NaBH_4$ + 6 M NaOH	Air	25	6	40 [83]	0.24	[19]
Pd/C (1 mg_{Pd} cm^{-2}) + CMSEBS55 + Nafion®, on Ni foam	Pt/C (1 mg_{Pt} cm^{-2})	N117	1.5 M $NaBH_4$ + 3 M KOH	15 wt% H_2O_2 + 1.5 M H_2SO_4	70	5	300 [330]	300.0	[20]
C_{Ni}-S_{Pd}/PANI (1 mg cm^{-2})	Pt/C (0.5 mg_{Pt} cm^{-2})	Nafion	2 M NaOH + 1 M $NaBH_4$	0.5 M H_2SO_4 + 2 M H_2O_2	60	5	120.2 [182]	120.2	[21]
C_{Ni}-S_{Pd}/rGO (1 mg cm^{-2})							310.2 [249]	310.2	
C_{Ni}-S_{Pd}/rGP1) (1 mg cm^{-2})							339.1 [279]	339.1	
Ni@Pt/MWCNT (1.0 mg cm^{-2}) + Nafion®	Pt/C (0.5 mg_{Pt} cm^{-2})	N117	2 M NaOH + 1 M $NaBH_4$	0.5 M H_2SO_4 + H_2O_2	60	5	162.6 [162]	162.6	[22]
Ni@Pd/MWCNT (1.0 mg cm^{-2}) + Nafion®							246.8 [225]	246.8	
Ni@Ru/MWCNT (1.0 mg cm^{-2}) + Nafion®							119.6 [112]	119.6	

CCH: chitosan chemical hydrogel binder; rGO: reduced graphene oxide, PANI: pure polyaniline, rGP: mixture of rGO and PANI; MWCNT: multi walled carbon nanotubes;

NRE212, NRE211, N112, N212, N117 are types of Nafion® cation-exchange membranes (DuPont); CS is a chitosan-based polymer electrolyte membrane; PFM is a polymer fiber membrane

References

(1) Moulder, J. F.; Chastain, J. *Handbook of X-Ray Photoelectron Spectroscopy: A Reference Book of Standard Spectra for Identification and Interpretation of XPS Data*; Physical Electronics Division, Perkin-Elmer Corporation, 1992.

(2) Machado, S. A. S.; Avaca, L. A. The Hydrogen Evolution Reaction on Nickel Surfaces Stabilized by H-Absorption. *Electrochim. Acta* **1994**, *39*, 1385–1391.

(3) Braesch, G.; Bonnefont, A.; Martin, V.; Savinova, E. R.; Chatenet, M. Borohydride Oxidation Reaction Mechanisms and Poisoning Effects on Au , Pt and Pd Bulk Electrodes : From Model (Low) to Direct Borohydride Fuel Cell Operating (High) Concentrations. *Electrochim. Acta* **2018**, *273*, 483–494.

(4) Li, H.; Li, H.; Dai, W. L.; Wang, W.; Fang, Z.; Deng, J. F. XPS Studies on Surface Electronic Characteristics of Ni-B and Ni-P Amorphous Alloy and Its Correlation to Their Catalytic Properties. *Appl. Surf. Sci.* **1999**, *152*, 25–34.

(5) Schreifels, J. A.; Maybury, P. C.; Swartz Jr., W. E. X-Ray Photoelectron Spectroscopy of Nickel Boride Catalysts: Correlation of Surface States with Reaction Products in the Hydrogenation of Acrylonitrile. *J. Catal.* **1980**, *65*, 195–206.

(6) Legrand, J.; Taleb, A.; Gota, S.; Guittet, M. J.; Petit, C. Synthesis and XPS Characterization of Nickel Boride Nanoparticles. *Langmuir* **2002**, *18*, 4131–4137.

(7) Zhang, D.; Cheng, K.; Shi, N.; Guo, F.; Wang, G.; Cao, D. Nickel Particles Supported on Multi-Walled Carbon Nanotubes Modified Sponge for Sodium Borohydride Electrooxidation. *Electrochem. commun.* **2013**, *35*, 128–130.

(8) Santos, D. M. F.; Eugénio, S.; Cardoso, D. S. P.; Šljukić, B.; Montemor, M. F. Three-Dimensional Nanostructured Ni–Cu Foams for Borohydride Oxidation. *Russ. J. Phys. Chem. A* **2015**, *89*, 2449–2454.

(9) Grinberg, V. A.; Mayorova, N. A.; Korlyukov, A. A.; Pasynskii, A. A. Direct Borohydride Oxidation Electrocatalysts Based on Ni–Ru/C and Ni–Ru–F/C Alloys. *Russ. J. Electrochem.* **2010**, *46*, 1289–1296.

(10) Saha, S.; Ganguly, S.; Banerjee, D.; Kargupta, K. Novel Bimetallic Graphene-Cobalt-Nickel (G-Co-Ni) Nano-Ensemble Electrocatalyst for Enhanced Borohydride Oxidation. *Int. J. Hydrogen Energy* **2015**, *40*, 1760–1773.

(11) Geng, X.; Zhang, H.; Ye, W.; Ma, Y.; Zhong, H. Ni-Pt/C as Anode Electrocatalyst for a Direct Borohydride Fuel Cell. *J. Power Sources* **2008**, *185*, 627–632.

(12) Song, C.; Wang, G.; Li, B.; Miao, C.; Ma, K.; Zhu, K.; Cheng, K.; Ye, K.; Yan, J.; Cao, D.; et al. A Novel Electrode of Ternary CuNiPd Nanoneedles Decorated Ni Foam and Its Catalytic Activity toward NaBH4 Electrooxidation. *Electrochim. Acta* **2019**, *299*, 395–404.

(13) Li, S.; Shu, C.; Chen, Y.; Wang, L. A New Application of Nickel-Boron Amorphous Alloy Nanoparticles: Anode-Catalyzed Direct Borohydride Fuel Cell. *Ionics* **2018**, *24*, 201–209.

(14) Ma, J.; Sahai, Y.; Buchheit, R. G. Evaluation of Multivalent Phosphate Cross-Linked Chitosan Biopolymer Membrane for Direct Borohydride Fuel Cells. *J. Power Sources* **2012**, *202*, 18–27.

(15) Choudhury, N. A.; Ma, J.; Sahai, Y. High Performance and Eco-Friendly Chitosan Hydrogel Membrane Electrolytes for Direct Borohydride Fuel Cells. *J. Power Sources* **2012**, *210*, 358–365.

(16) Ma, J.; Sahai, Y.; Buchheit, R. G. Direct Borohydride Fuel Cell Using Ni-Based Composite Anodes. *J. Power Sources* **2010**, *195*, 4709–4713.

(17) Liu, B. H.; Li, Z. P.; Suda, S. Development of High-Performance Planar Borohydride Fuel Cell Modules for Portable Applications. *J. Power Sources* **2008**, *175*, 226–231.

(18) Cheng, H.; Scott, K.; Lovell, K. Material Aspects of the Design and Operation of Direct Borohydride Fuel Cells. *Fuel Cells* **2006**, *6*, 367–375.

(19) Liu, B. H.; Li, Z. P.; Arai, K.; Suda, S. Performance Improvement of a Micro Borohydride Fuel Cell Operating at Ambient Conditions. *Electrochim. Acta* **2005**, *50*, 3719–3725.

(20) Wang, Z.; Parrondo, J.; He, C.; Sankarasubramanian, S.; Ramani, V. Efficient PH-Gradient-Enabled Microscale Bipolar Interfaces in Direct Borohydride Fuel Cells. *Nat. Energy* **2019**, *4*, 281–289.

(21) Mahmoodi, R.; Hosseini, M. G.; Rasouli, H. Enhancement of Output Power Density and Performance of Direct Borohydride-Hydrogen Peroxide Fuel Cell Using Ni-Pd Core-Shell Nanoparticles on Polymeric Composite Supports (rGO-PANI) as Novel Electrocatalysts. *Appl. Catal. B Environ.* **2019**, *251*, 37–48.

(22) Hosseini, M. G.; Mahmoodi, R. Improvement of Energy Conversion Efficiency and Power Generation in Direct Borohydride-Hydrogen Peroxide Fuel Cell: The Effect of Ni-M Core-Shell Nanoparticles (M = Pt, Pd, Ru)/Multiwalled Carbon Nanotubes on the Cell Performance. *J. Power Sources* **2017**, *370*, 87–97.